Adsorption 4, 25–33 (1998)

Adsorption of SO_2 from Wet Mixtures on Hydrophobic Zeolites

SABINA A. ROUF AND MLADEN EIĆ
Department of Chemical Engineering, University of New Brunswick, Fredericton, NB E3B 5A3, Canada

Received July 15, 1996; Revised February 7, 1997; Accepted April 8, 1997

Abstract. Breakthrough curve measurements of SO_2 and water vapor were carried out on a number of selected mordenite and pentasil zeolites from their binary and ternary mixtures with CO_2 at 50 and 100°C. SO_2 capacities of these samples were found to be significantly reduced by the presence of water. Competitive adsorption led to unusually high overshoot peaks of SO_2 breakthrough curves. On the other hand, SO_2 was found to displace water on the samples with very high silica to alumina ratio. A linear driving force, isothermal model was used to predict the breakthrough curves. Langmuir and extended Langmuir equilibrium models were used to describe the equilibrium properties of water and SO_2, respectively. The overall mass transfer resistance obtained from the model was compared to the values calculated from a simplified biporous adsorbent model to shed some light on the adsorption kinetics.

Keywords: hydrophobic zeolites, breakthrough curves, adsorption, binary mixtures, modeling, overall mass transfer, roll-up

Introduction

Silica rich zeolites are hydrophobic in nature and therefore are expected to possess high capacity and selectivity for SO_2 adsorption in the presence of water vapor. The objective of this work was focused on the study of SO_2 and H_2O adsorptive behavior in their binary mixtures on mordenite and pentasil zeolites (MOR and MFI types) over a wide range of SiO_2/Al_2O_3 molar ratios (11–350). Compositions of the mixtures were varied from 1.4 to 5 vol% H_2O and 500–1800 ppmv SO_2. A limited study involving ternary mixture with CO_2 was also carried out. Breakthrough and adsorption equilibrium experiments were used to determine basic kinetic and equilibrium parameters. This paper will specifically address SO_2 roll-up effect (Young, 1987) which occurs as a result of displacement of weaker adsorbed species (SO_2) with more strongly adsorbed species (H_2O). The effect can be used as an alternative means to concentrate SO_2 in the exit stream. Mathematical analysis based on the linear driving force model was employed to predict breakthrough curves with roll-up effect in the binary mixtures.

Experimental

Breakthrough measurements were carried out using a packed column (9 cm in length and 1 cm in i.d.) and recording the concentration of each component at the outlet of the column as a function of time. Gas streams containing varying concentrations of SO_2 (1800, 950 and 500 ppmv) and water (5%, 3% and 1.4% by volume) were used for breakthrough measurements at 50 and 100°C and atmospheric pressure. A flow rate of 150 sccm/min was maintained through the column. Concentrations of SO_2 and water at the column outlet were measured with an IR SO_2 analyzer and a standard thermal conductivity detector (TCD), as shown in Fig. 1. The effluent gas from the column was passed through a selective Haysep D column before entering the detectors. The adsorbed species in this column were eluted at different times which provided the basis for the effluent analysis. Nitrogen was used as the carrier gas for all gas mixtures. A ternary gas mixture was prepared by introducing CO_2 in the original, binary mixture. A CO_2 breakthrough curve in the ternary mixture could not be obtained due to interference of its peak

Table 1. List of zeolite samples used in the study.

Zeolite structure	Company/ commercial name	SiO_2/Al_2O_3 (molar ratio)	Average pellet size (cm)	Mean macropore diameter (μm)
MOR (Na-mordenite)	PQ Corporation CP 500-11	11	0.178	—
MOR (H-mordenite)	PQ Corporation MOR 20A	20	0.178	0.2
MOR (H-mordenite)	PQ Corporation MOR 30A	35	0.178	—
MFI (H-ZSM-5)	PQ Corporation CBV 3010	26	0.178	0.2
MFI (H-ZSM-5)	PQ Corporation CBV 5020	43	0.178	—
MFI (H-ZSM-5)	Union Carbide SA-5	150	0.178	0.75

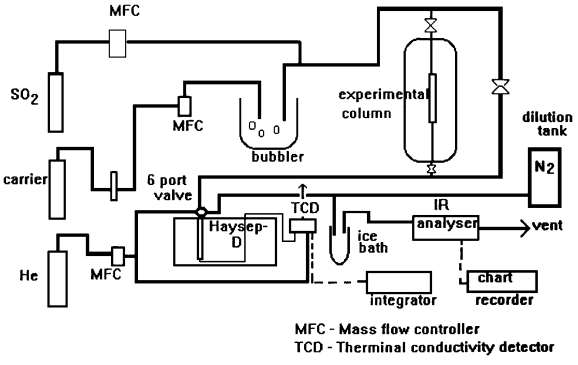

Figure 1. Experimental settings for measurement of breakthrough curves.

with nitrogen. The samples were regnerated by heating at 330°C for 12 hours under a flow of nitrogen before each run. The pellet density and mean macropore size for selected samples were determined by mercury porosimetry. The samples for this experiment were supplied by PQ Corporation and Union Carbide. The properties of the samples are presented in Table 1.

Theory

Equilibrium

The equilibrium capacity of the samples can be calculated from a simple mass balance of the column based on the stoichiometric time t^*,

$$t^* = \frac{L}{v}\left[1 + \frac{(1-\epsilon)}{\epsilon}\frac{q^*}{C_0}\right] \tag{1}$$

where t^*, stoichiometric time can be calculated from the breakthrough curve (first moment analysis):

$$t^* = \int_0^\infty (1 - C/C_0)\, dt \tag{2}$$

Column Dynamics and Modeling of Breakthrough Curves

Differential mass balance for an adsorption column under an axially-dispersed plug flow pattern for a trace system has the following form:

$$-D_L \frac{\partial^2 C_i}{\partial Z^2} + v\frac{\partial C_i}{\partial Z} + \frac{\partial C_i}{\partial t} + \frac{(1-\epsilon)}{\epsilon}\frac{\partial q_i}{\partial t} = 0 \tag{3}$$

The following set of initial and boundary conditions can be applied to the system (Wehner and Wilhem, 1956; Raghavan et al., 1985):

$$\begin{aligned} C_i(z,0) &= 0 \\ q_i(z,0) &= 0 \end{aligned} \tag{4}$$

and at $t \geq 0$,

$$D_L\left(\frac{\partial C_i}{\partial Z}\right)_{z=0} = -v[(C_i)_{z=0^-} - (C_i)_{z=0}] \tag{5}$$

and

$$\left(\frac{\partial C_i}{\partial Z}\right)_{z=L} = 0 \tag{6}$$

The axial dispersion coefficient (D_L) for the mass balance equation was calculated from the Edwards and

Richardson correlation (1968):

$$\frac{D_L}{2vR_p} = \gamma_1 \frac{D_m}{2vR_p} + \frac{1}{\mathrm{Pe}_\infty \frac{1+\beta\gamma_1 D_m}{2vR_p}} \tag{7}$$

with $\gamma_1 = 0.73$, $\beta = 13.0$ and $\mathrm{Pe}_\infty = 2.0$.

Mass transfer between fluid and solid phase was expressed in terms of a linear driving force model:

$$\frac{\partial q}{\partial t} = k(q^* - q) \tag{8}$$

The overall mass transfer coefficient (k) in the above expression can be correlated to film, macropore and micropore resistance by a simplified biporous adsorbent model for the pellet (Ruthven, 1984).

$$\frac{1}{kK} = \frac{R_p}{2k_f} + \frac{R_p^2}{15\epsilon_p D_e} + \frac{r_c^2}{15K D_c} \tag{9}$$

where

$$D_e = \frac{D_p}{\tau} \tag{9a}$$

Finally, the equilibrium relationship for a mixture can be expressed as:

$$q_i^* = f_i(C_1, C_2, \ldots, C_N) \tag{10}$$

or

$$q_i^* = f_i'(p_1, p_2, \ldots, p_N),$$

which in this case was expressed in terms of the extended Langmuir equilibrium model:

$$\frac{q_i^*}{q_s} = \frac{b_i p_i}{1 + \sum b_i p_i} \tag{11}$$

The above equations adequately describe the system under isothermal conditions.

Results and Discussion

Binary Mixture

The binary mixture containing 1800 ppmv SO_2 and 5% water by volume was considered the original binary mixture. The other binary mixtures, obtained by varying the concentration of either SO_2 or water, were designated as binary mixtures a, b, c and d, as listed in Table 2.

Table 2. Composition of different gas mixtures.

Mixture	SO_2 ppmv	H_2O vol%	CO_2 vol%	Temperature °C
Binary mixture	1800	5	—	50
Ternary mixture	1800	5	9	50
Binary mixture a	950	5	—	50
Binary mixture b	500	5	—	50
Binary mixture c	1800	3	—	50
Binary mixture d	1800	1.4	—	50
Binary mixture e	1800	5	—	100

Water Breakthrough Curves

Selected water and SO_2 breakthrough curves on mordenite ($SiO_2/Al_2O_3 = 20$) in the original binary mixture are shown in Fig. 2. All water breakthrough curves obtained on mordenite and ZSM-5 samples used in this study were S-shaped (Rouf, 1995). Water was present at a much higher concentration compared to SO_2 in the binary mixtures and its breakthrough behavior implies that it was more strongly adsorbed than SO_2 on these samples (water breakthrough occurred after SO_2). A different breakthrough behavior was observed on silicalite (i.e., on samples with very high silica to alumina ratio). An earlier breakthrough of water compared to SO_2 and a small overshoot in its breakthrough curve was observed on these samples (Rouf, 1995). The nature of adsorption interactions changed from the strong electrostatic to weak van der Waals forces as the silica to alumina ratio increased in the sample; this facilitated the adsorption of SO_2 because of its higher polarizability compared to water.

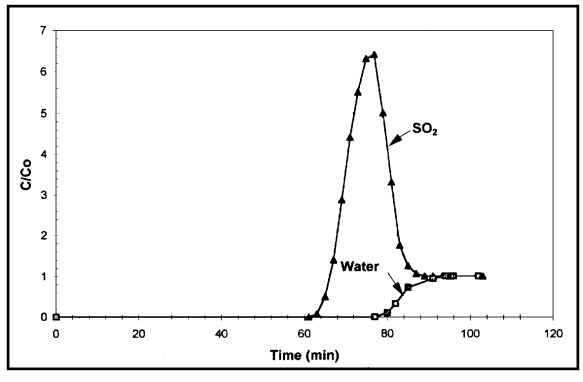

Figure 2. SO_2 and water vapor breakthrough curves for original binary mixture on mordenite 20 sample.

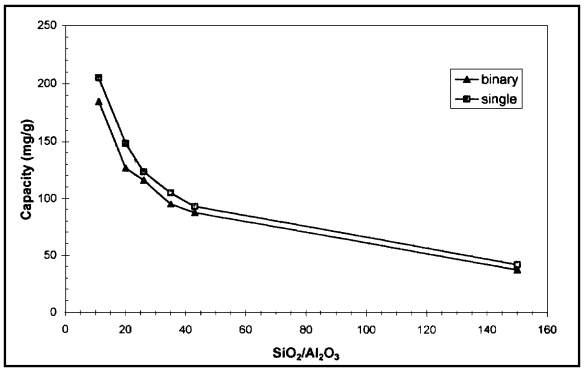

Figure 3. Equilibrium capacities of water vapor at 50°C for single component and binary mixture containing 3 vol% water.

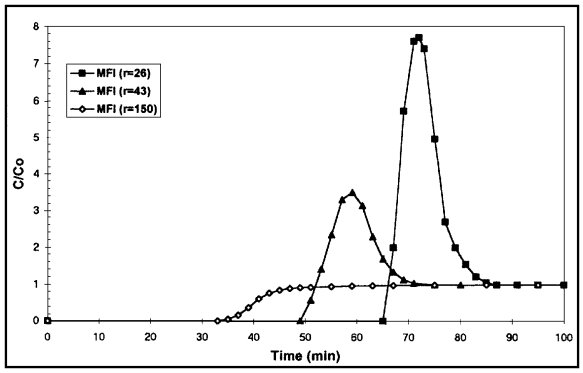

Figure 4. SO_2 breakthrough curves for original binary mixture on different MFI samples.

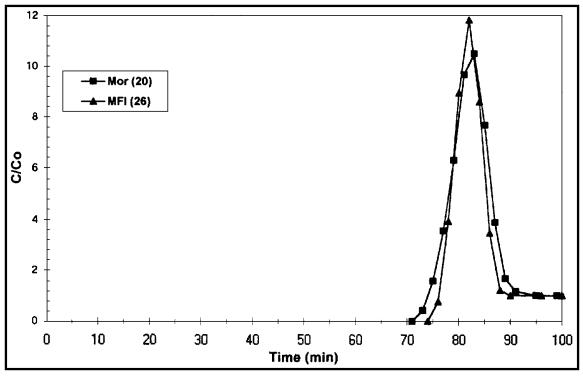

Figure 5. SO_2 breakthrough curves for binary mixture (a) on MOR 20 and MFI 26 samples.

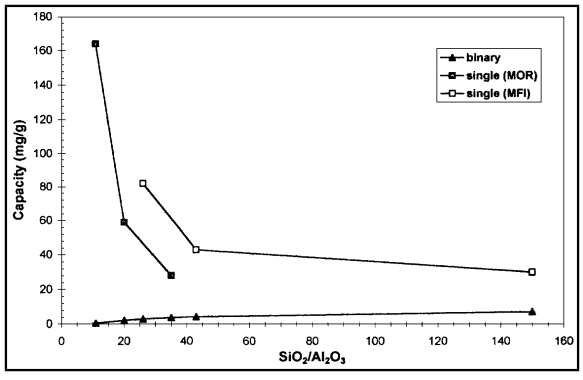

Figure 6. Equilibrium capacities of SO_2 at 50°C for single component and binary mixture containing 2,000 ppmv SO_2.

Water equilibrium capacities in the original binary mixture were plotted as a function of silica to alumina ratio in the sample (Fig. 3). They decreased with increasing silica to alumina ratio (i.e., increasing hydrophobicity) irrespective of the structure. A small reduction in capacity was observed when the binary capacities were compared with the single component water capacities on these samples (Fig. 3). This suggests that the adsorption of water was not significantly affected by the presence of SO_2 in the binary mixture. A similar trend in water breakthrough was also observed on these samples with the other gas mixtures (a–d)(Rouf, 1995).

SO_2 Breakthrough Curves

Original Mixture. SO_2 breakthrough curves in the original binary mixtures showed an overshooting shape on all mordenite and ZSM-5 samples investigated in this study (Fig. 2). The almost complete displacement of SO_2 by water resulted in unusually high overshoot peaks which reached concentrations of 3 to 12 times the inlet concentration. Such high roll-up effects are not a common phenomena in the adsorption of multicomponent mixtures. The height of the overshoot peak was found to decrease as the silica to alumina ratio was increased in the samples; the peak ultimately disappeared on silicalite (Fig. 4) due to the stronger adsorption of SO_2 on high silica zeolites where van der Waals forces were dominant. As for the zeolite structure, higher overshoots were generally observed in ZSM-5 than on mordenite (Fig. 5). This may have been due to the less restrictive, two-dimensional channel structure of ZSM-5, which allowed easier displacement and desorption of SO_2 molecules than in mordenite.

SO_2 equilibrium capacities in the original binary mixture were plotted as a function of the silica to alumina ratio in Fig. 6. Results show that SO_2 equilibrium

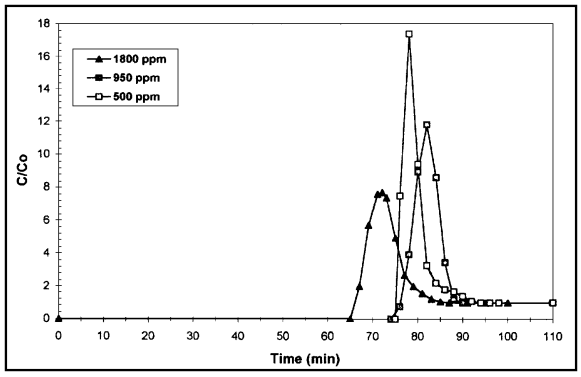

Figure 7. SO_2 breakthrough curves for binary mixtures (a) and (b) in comparisons with the original mixture on MOR 20 sample.

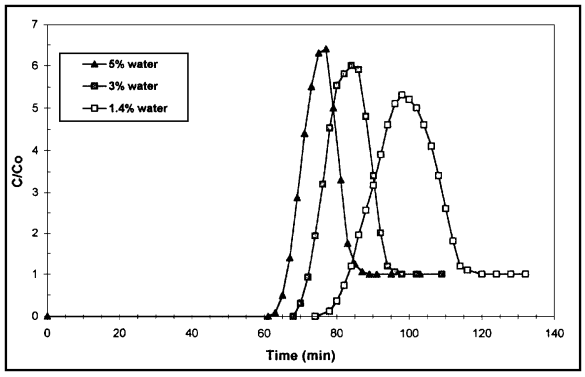

Figure 8. SO_2 breakthrough curves for binary mixtures (c) and (d) in comparisons with the original mixture on MOR 20 sample.

capacity increases with increasing silica to alumina ratio and reaches a maximum on silicalite, which is indicative of a relative increase when compared to the water capacities for same systems. Contrary to this the single component SO_2 capacities show a decreasing trend similar to the results shown for water. When compared with the single component SO_2 capacities, a drastic reduction in SO_2 equilibrium capacities was observed due to the presence of water. This reduction in capacity was also observed by other investigators in previous studies (Tantet, 1993; Gariepy and Zwiebel, 1971).

Binary Mixtures a and b. These mixtures had the same concentration of water as the original binary mixture (5% by vol.) but lower concentration of SO_2 (950 and 500 ppm respectively). Selected SO_2 breakthrough curves in these mixtures on the mordenite sample are presented in Fig. 7, along with the breakthrough curve in the original binary mixture for the comparisons. It appears from this figure that lowering the concentration of SO_2 results in a higher overshoot of SO_2 on these samples. This type of behavior was predicted by Gariepy and Zwiebel (1971) and observed by Stenger et al. (1993) for SO_2-water-mordenite systems. The increasing overshoot results from the relative competition for adsorption sites between the sorbate molecules. Water can more easily displace SO_2 if the latter is present at the lower concentrations.

Binary Mixtures c and d. The SO_2 concentration was kept the same in these mixtures as in the original binary mixture (1800 ppmv), but the concentration of water was decreased from 5% by volume to 3% (mixture c) and then to 1.4% (mixture d). Figure 8 shows the SO_2 breakthrough curves in these mixtures on the mordenite sample in comparison to the original mixture. The SO_2 overshoot peak height was found to decrease with decreasing water concentration in the feed, as was found in the previous studies (Gariepy and Zwiebel, 1971; Stenger et al., 1993). The relative competition between SO_2 and water increases as water vapor concentration is increased. At higher concentrations water has a greater competitive edge and can easily displace more SO_2, resulting in the higher overshoot peaks.

Binary Mixture e. This mixture has the same composition as the original binary mixture except adsorption was carried out at 100°C instead of 50°C. The SO_2 breakthrough curve under this condition is compared to that in the original binary mixture in Fig. 9. Since adsorption is an exothermic process, the breakthrough time decreased significantly with increasing

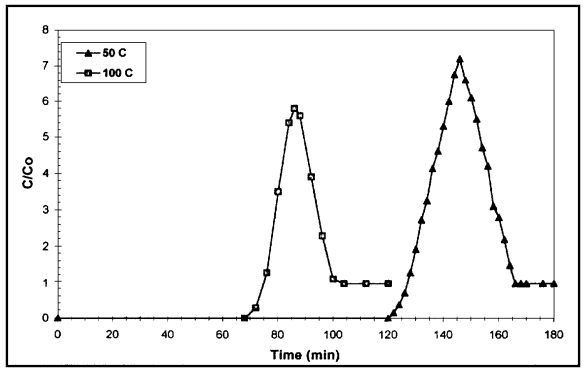

Figure 9. SO_2 breakthrough curves for original and binary mixture (e) on MOR 11 sample.

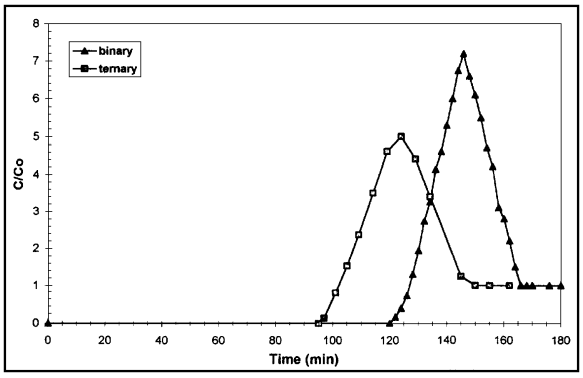

Figure 10. SO_2 breakthrough curves for original and ternary mixture on MOR 11 sample.

adsorption temperature. The overshoot peak also decreased but still exhibited a high value. Similar results were obtained by Stenger et al. (1993), who carried out experiments at 50, 100 and 150°C.

Ternary Mixture

This mixture contained CO_2 (9% by vol.) in addition to the gases present in the original binary mixture. The SO_2 breakthrough curves in the ternary and original binary mixtures are presented in Fig. 10. The SO_2 capacity of the mordenite sample was only moderately reduced by the presence of CO_2 in the gas mixture. The relatively small effect of CO_2 co-adsorption is mainly due to the lower polarity of CO_2 compared to SO_2 and water molecules and therefore lower adsorption affinity. Similar moderate effects of CO_2 were observed in a number of previous studies (Tantet, 1993; Gariepy and Zwieble, 1971; Stenger et al., 1993; Roux et al., 1973).

Modeling of the Breakthrough Curve

The model was obtained by solving Eqs. (3), (8) and (10) with the accompanying initial and boundary conditions (Eqs. (4)–(6)) by the numerical orthogonal collocation method. The small dimensions of the experimental column (length 9 cm, i.d. 1 cm) and the low heat of adsorption of water on the hydrophobic zeolite justified the assumption of the isothermal condition (Rouf, 1995). To shed some light on the adsorption kinetics the experimental values of the overall mass transfer resistance ($1/kK$), obtained by matching the theoretical with the experimental curve, were compared with those calculated from the biporous adsorbent model, Eq. (9). The third term in Eq. (9), which represents micropore resistance, was neglected in this analysis due to the small crystal size of the samples (1–2 μm), as well as assuming high values of the KD_c product for both SO_2 and water adsorption systems. The Wakao and Funazkri correlation was used to estimate the external film mass transfer coefficient required for the calculation of external film resistance. An average value of 3 was used for the tortuosity factor (τ) in the calculation of effective diffusivity (Tantet et al., 1995).

Water Breakthrough Curves

The water equilibrium capacity and breakthrough curves were found to be only slightly affected by the presence of SO_2 in the binary mixture. For this reason, the presence of SO_2 was ignored and the system was treated as a single component. Water isotherms gave an excellent fit to the Langmuir equilibrium model (Tantet et al., 1995). Figure 11 compares the selected theoretical and experimental water breakthrough curves on mordenite ($SiO_2/Al_2O_3 = 20$) from the original binary mixture. The overall mass transfer coefficient (k), obtained by matching the theoretical curve with the experimental data for the single component systems, was combined with equilibrium constant K to calculate the overall mass transfer resistance ($1/kK$). These values were compared with the calculated ones using biporous model (Eq. (9)). A summary of these comparisons for water systems is given in Table 3(a). Details of the calculation are given in (Tantet et al., 1995). The discrepancy between the values suggests

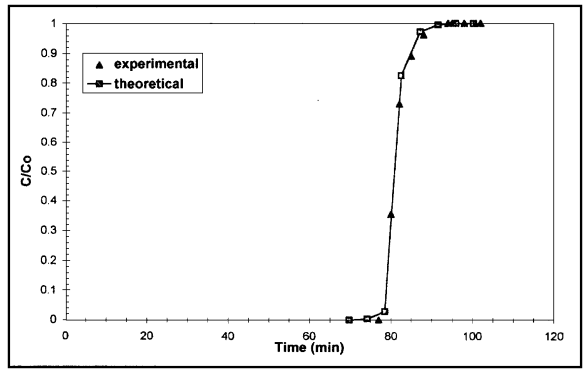

Figure 11. Modeling of water vapor breakthrough curve for binary mixture (b) on MFI 26 sample.

Table 3a. Comparison of experimental and calculated mass transfer resistances for water on MOR (20) and MFI (26) samples at 50°C.

Sample	Macropore resistance (1)	Fluid film resistance (2)	Overall resistance (1) + (2)	Overall resistance (from exper. data)
	$R_p^2/15\epsilon_p D_p$ (s)	$R_p/3k_f$ (s)	$1/kK$ (s)	$1/kK$ (s)
		MOR (20)		
5% water	0.032	0.007	0.039	0.104
3% water	0.032	0.007	0.039	0.094
1.4% water	0.032	0.007	0.039	0.056
		MFI (26)		
5% water	0.030	0.007	0.037	0.083
3% water	0.030	0.007	0.037	0.077
1.4% water	0.030	0.007	0.037	0.051

a significant contribution from surface diffusion in the macropors, in particular for MOR-20 sample. This explanation becomes more plausible for the higher water vapor concentration levels (3 and 5 vol%). These concentration conditions, when combined with relatively low temperature (50°C), could cause adsorption on the macropore surface due to capillary condensation, ultimately leading to the surface diffusion. From the results shown in Table 3(a) it is evident that the best agreement between the experimental and calculated results is at the lowest water concentration (1.4%), where the effects of surface diffusion are expected to be least significant. Mass transfer resistance ($1/kK$) values for MFI-26 are smaller, due to generally lower adsorption capacity of that sample in comparison with MOR-20. Consequently, contributions of the surface diffusion are less significant, though far from being negligible (differences between the experimental and calculated data are still very notable, particularly at the higher water vapor concentration levels). To explore this hypothesis further, it is necessary to carry out equilibrium and pore diffusivity measurements at higher temperatures where the effects of surface diffusion will be negligible.

Another source that may contribute to this discrepancy was the use of the value of 3 for the tortuosity factor for the water diffusion. Further experimental investigation, involving kinetic measurements to determine effective diffusion in the zeolite particles is necessary to warrant the values of tortuosity factor in this study.

SO_2 Breakthrough Curves

Modeling parameters of this system were derived from kinetic and equilibrium data of the single component SO_2 system (Tantet et al., 1995). The equilibrium relationship in the binary mixture was represented by the extended Langmuir model. The experimental and theoretical values (Eq. (9)) of the overall mass transfer coefficient for SO_2 are compared in Table 3(b). Excellent agreement between these values confirmed the validity of biporous model and the assumptions used for the mass transfer of SO_2. Table 3(b) also shows that macropore diffusion is a predominant step in the process. Figure 12 compares the experimental and predicted SO_2 breakthrough curves in the original binary mixture on mordenite ($SiO_2/Al_2O_3 = 20$). The theoretical breakthrough curve is in a close agreement with the experimental curve. The model also correctly predicts a trend for mixtures a–d (a higher overshoot with a lower concentration of SO_2 in the

Table 3b. Comparison of experimental and calculated mass transfer resistances for SO_2 (1800 ppm SO_2 and 5% water by volume, $T = 50$°C) on different samples.

Sample	Macropore resistance (1)	Fluid film resistance (2)	Overall resistance (1) + (2)	Overall resistance (from exper. data)
	$R_p^2/15\epsilon_p D_p$ (s)	$R_p/3K_f$ (s)	$1/kK$ (s)	$1/kK$ (s)
MOR (20)	0.029	0.006	0.035	0.036
MFI (26)	0.026	0.006	0.032	0.033
MFI (150)	0.018	0.006	0.024	0.025

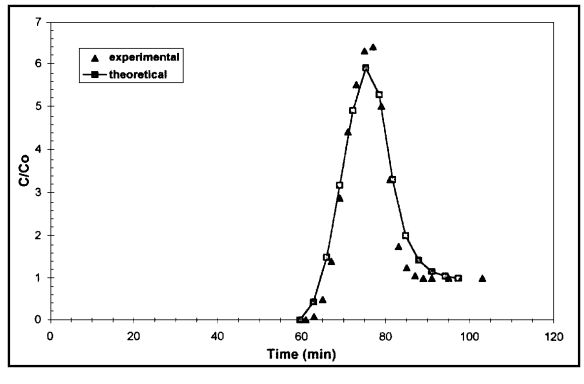

Figure 12. Modeling of SO_2 breakthrough curve for original binary mixture on MOR 20 sample.

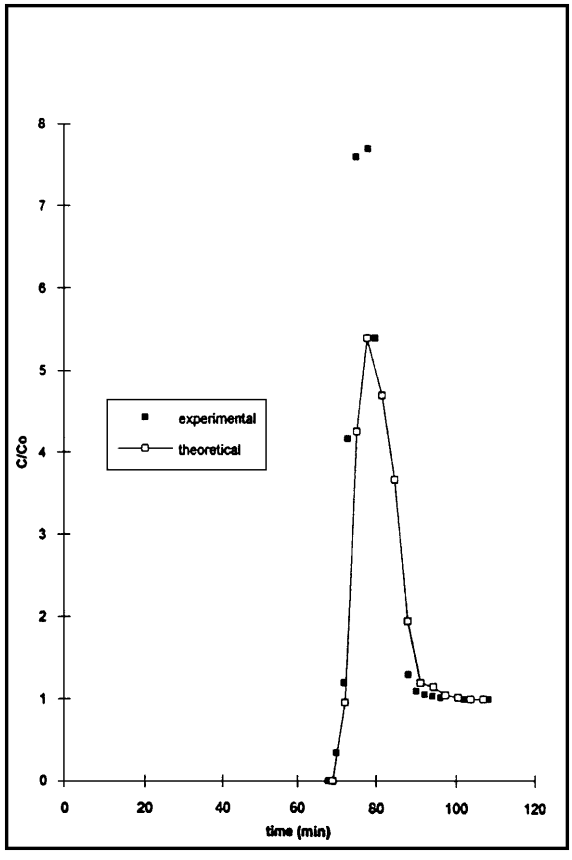

Figure 13. Modeling of SO_2 breakthrough curve for binary mixture (c) on MFI 26 sample.

feed mixture and lower overshoot with lower concentration of water (Rouf, 1995)). However, in these mixtures the heights of the overshoot peak were underpredicted (Rouf, 1995), (Fig. 13). The difference could be attributed to the insufficiency of the Langmuir model used, particularly in the lower concentration region.

Conclusion

Coadsorption of water with SO_2 drastically reduced the single component SO_2 capacity of the zeolite samples. Competitive adsorption in the binary mixture led to the unusually high water-driven overshoot peak in the SO_2 breakthrough curve. The overshoot peak increased in height with decreasing SO_2 and increasing water concentration in the feed mixture. In contrast, co-adsorption of CO_2 had only a moderate effect on the breakthrough behavior of water and SO_2. The breakthrough model correctly predicted experimental curves for both water and SO_2 in their binary mixtures. Bi-porous adsorbent model correctly described mass transfer of SO_2 for all the samples used in the study.

The high overshoot peaks of SO_2 can be used to concentrate and separate SO_2 as suggested in previous studies (Gariepy and Zwiebel, 1971; Roux et al., 1973). The overshoot peaks on the samples investigated in this study were found to be much higher than those observed in the earlier studies. There is a potential of a large increase of SO_2 concentration at the effluent from the adsorption column, thus increasing efficiency of the SO_2 removal in a conventional scrubbing unit.

Nomenclature

b	Langmuir adsorption constant, atm^{-1}
C, C_0	Effluent and inlet sorbate concentration in the gas phase, $kmol/m^3$
D_c, D_e	Intracrystalline diffusivity and effective macropore diffusivity, m^2/s
D_L	Axial dispersion coefficient, m^2/s
D_p	Pore diffusivity, m^2/s
K	Equilibrium constant, dimension less
L	Length of column, m
k	Overall effecitve film mass transfer coefficient, s^{-1}
k_f	External fluid film mass transfer coefficient, m/s
q^*	Equilibrium capacity of the adsorbent, $kmol/m^3$
q	Sorbate concentration in solid phase, $kmol/m^3$
q_s	Limiting saturation concentration in the solid phase, $kmol/m^3$
p	Partial pressure of sorbate, atm
R	Gas constant, g/kmol K
R_p	Radius of adsorbent particle, m
r_c	Radius of single crystal, m
t^*	Stoichiometric time, s
v	Interstitial velocity of gas, m/s
Z	Distance measured from column inlet, m
Pe_∞	Limiting value of Peclet number (Pe) as $Re \to \infty$
β_i, γ_i	Coefficients in Eq. (7)
ϵ, ϵ_p	Bed voidage and porosity of pellet
τ	Tortuosity factor

Acknowledgments

Financial support from the Natural Sciences and Engineering Research Council of Canada (NSERC)

and Commonwealth Scholarship Fund are greatfully acknowledged.

References

Edwards, M.F. and J.F. Richardson, *Chem. Eng. Sci.*, **23**, 109 (1968).

Gariepy, R.L. and I. Zwiebel, *AIChE Symp. Ser.*, **117**, 67 (1971).

Raghavan, N.S., M.M. Hassan, and D.M. Ruthven, *AIChE J.*, **31**(3), 385 (1985).

Rouf, S., M.Sc. Thesis, University of New Brunswick, Canada, 1995.

Roux, A.J., A.A. Huang, Y.H. Ma, and I. Zwiebel, *AIChE Symp. Ser.*, **69**, 134, 46 (1973).

Ruthven, D.M., *Principles of Adsorption and Adsorption Processes*, pp. 242–245, John Wiley and Sons, New York, 1984.

Stenger, H.G., K. Hu, and D.R. Simpson, *Ind. Eng. Chem. Res.*, **32**, 2736 (1993).

Tantet, J., M.Sc. Thesis, University of New Brunswick, Canada, 1993.

Tantet, J., M. Eić, and R. Desai, *Gas Separation and Purification*, **9** (3), 213 (1995).

Wehner, J.F. and R.H. Wilhem, *Chem. Eng. Sci.*, **6**, 89 (1956).

Young, R.T., *Gas Separation by Adsorption Processes*, Chapter 5, Butterworth Publishers, Stoneham, MA, 1987.